31st Annual International Conference of the IEEE EMBS
Minneapolis, Minnesota, USA, September 2-6, 2009

MR-guidance of HIFU Therapy

Kim Butts Pauly, *Member IEEE*, Viola Rieke, Andrew B. Holbrook, Will Grissom, Jean Chen, Elena Kaye

***Abstract*—MR guidance of high intensity focused ultrasound is evolving with each new application. In this paper we describe ongoing research in the MR-guidance aspect of MR-guided focused ultrasound. The structure is divided into the pretreatment/setup phase of the procedure, MR thermometry for monitoring the actual treatment, and methods for assessment and follow-up.**

I. Introduction

MAGNETIC resonance guided focused ultrasound (MRgFUS) is a promising technique for a number of clinical indications. It is currently FDA approved for the treatment of uterine fibroids and is being investigated for treatments in the prostate, liver, breast, and brain. The roles of image guidance are to target the therapy, monitor the progress of the therapy, and assess its effectiveness. Magnetic resonance imaging (MRI) is well suited to perform all three of these roles. The soft tissue contrast needed for targeting many of these treatments is outstanding. Guidance usually takes the form of monitoring the tissue temperature, a powerful feature of MRI and important for ablative therapies. MRI is rich in contrast mechanisms, which can be exploited for assessing what was treated.

The basis for MR temperature imaging is that the hydrogen electrons shield the nucleus from the magnetic field, decreasing the resonant frequency of the protons. Hydrogen bonds normally existing between water molecules effectively pull electrons away from their protons, increasing the resonant frequency. But, as the temperature of the tissue rises, hydrogen bonds in the tissue stretch, bend, and break. Where this happens, the electrons increasingly shield the protons from the magnetic field, reducing the net field seen by the protons, and the overall resonant frequency. The effect has been shown to be the same for all aqueous tissues and linear within the temperature range of interest, with a temperature coefficient of α = -0.01 ppm/°C [1]-[3]. Use of this relationship to measure temperature is referred to as the proton resonant frequency shift (PRF) thermometry. In practice, the temperature change in tissue is found from the change in phase ϕ in a series of gradient echo images by the following relationship,

$$\Delta T = \frac{\phi - \phi_0}{\alpha \gamma B_0 T E} \quad (1)$$

where the echo time TE, the field strength B_0, and the gyromagnetic ratio γ are also known. To predict tissue damage from the ablation, the temperature-time course is often converted into thermal dose according to the Arrhenius-damage integral [4]. PRF thermometry is easily performed in stationary tissues and MR thermometry has become integral in focused ultrasound treatments in the United States [5]-[7]. An example set of images demonstrating MR thermometry is shown in Fig. 1.

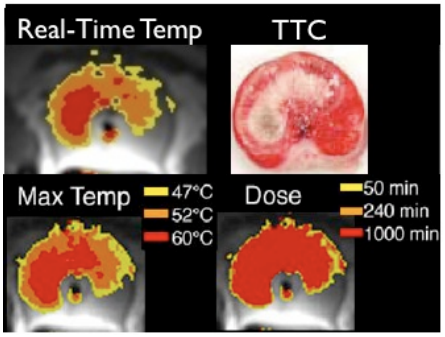

Fig. 1. A single real-time temperature image is shown, as is the maximum temperature achieved across the whole treatment and the resulting thermal dose map. The TTC image shows the heat fixed tissue and surrounding non-heat fixed coagulative necrosis that correlate well to the treatment area on the thermal dose maps.

MR-guided focused ultrasound is a fairly new field. As applications expand, there is a need to tailor techniques to suit the needs of each application. For example, MR thermometry as described above is very sensitive to motion artifacts, which is particularly relevant to applications in the abdomen. In this paper we describe ongoing research in the MR-guidance aspect of MR-guided focused ultrasound. This is divided into the pretreatment/setup phase of the procedure, MR thermometry for monitoring the actual treatment, and methods for assessment and follow-up.

II. Pretreatment/Setup

A. Requirements

The requirements for the pretreatment/setup phase of the procedure are not just to image the soft tissue in order to target the treatment, but also to ensure proper calibration and focusing of the equipment.

B. Non-Destructive Test Spot

Proper calibration of the focal spot location has been done with the application of a "test shot" with a temperature rise of only a few degrees. A temperature rise of less than 5°C

Manuscript received April 7, 2009. This work was supported by NIH Grants CA121163, CA111981, CA118276, and RR009784.

K Butts Pauly is with Stanford University (650-725-8551; fax: 650-723-5795; e-mail: kbpauly@ Stanford.edu). A. Holbrook is with Stanford University. (e-mail: aholbrook@stanford.edu). Viola Rieke is with Stanford University. (e-mail: vrieke@stanford.edu). Will Grissom is with Stanford University. (e-mail: wgrissom@gmail.com). Jing Chen was with Stanford University and is currently at the Institute of Biophysics in Bejing. (e-mail: jchen@bcslab.ibp.ac.cn).

allows visualization of the focal spot, without damaging the tissue. However, one concern with this approach is that there are applications in which a small temperature rise is not expected, such as in ultrasound enhanced drug delivery [8]-[11] or in blood brain barrier opening applications [12]-[15].

To visualize the focal spot, we and others are investigating the use of acoustic radiation force imaging with MR (MR-ARFI) [16]-[17]. Radiation pressure accompanies any wave and is proportional to the intensity I divided by the speed of the wave c,

$$F = \frac{2\alpha I}{c} \qquad (2)$$

where α is the absorption coefficient of the tissue. Since the resulting tissue displacement is proportional to the ultrasound amplitude, the focal spot can be rapidly visualized and localized, without a temperature rise.

An example setup for MR-ARFI is shown in Fig. 2. In the sequence, gradients are used such that tissue displacement is encoded in the image phase. While stationary spins are rephased, those that experienced the radiation force displacement have a net phase shift. The sequence is repeated with the displacement encoding gradients reversed and the phase difference between the two images is calculated. After some additional processing, the MR-ARFI image is proportional to displacement, an example of which is shown in Fig. 2. Images such as these could potentially be used to calibrate the equipment, without any temperature rise.

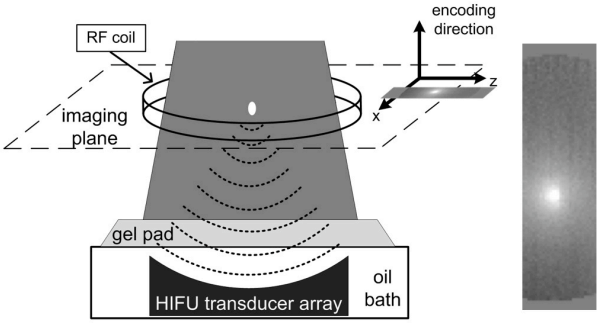

Fig. 2. (left) Example setup for MR-ARFI. Ultrasound is applied from below the phantom. The gel phantom at the focus experiences the radiation force in the beam direction, the y direction. Encoding gradients are applied along the same direction. (right) Example MR-ARFI image in which displacements are registered in the phase of the image, while stationary spins are refocused. Displacements in the focal spot measure about a micrometer.

C. Phase Aberration Correction in the Brain

The application of focused ultrasound in the brain requires correction for phase aberrations from the skull. The variable path length through the skull, in which the speed of sound is about double that of soft tissue, results in phase variations at the focal spot. If these are not corrected, the focal spot can be shifted and broadened, and even demonstrate multiple peaks [18].

Current corrections are based on calculations from a CT scan of the head from which the path length through the skull is estimated for all elements [18]. It would be desirable to avoid the high x-ray dose given to the patient from these high resolution scans and to eliminate the need for an additional scan, with the time and scheduling that that requires. It is possible that these calculations can be made from MR images of bone, acquired with ultrashort echo times (UTE) of a few microseconds [19]. Another possibility is that MR-ARFI could be used to focus the beam, in methods similar to those demonstrated with ultrasound [20].

III. Real-time Monitoring with MR Thermometry

A. Limitations

In PRF thermometry, a subtraction of the baseline phase is performed in order to eliminate any contribution to the phase from sources such as magnetic inhomogeneities. Only the *change* in phase is attributed to temperature. A major limitation of MR thermometry results from motion of moving organs, such as the liver and heart, which results in misregistration of the baseline and heating images. In addition, feedback of the organ position or progress of therapy can improve the control of the ultrasound. These are areas of current research described in more detail here.

B. Multibaseline Subtraction Methods

In the most common processing method for MR thermometry, called baseline subtraction, it is critical that the pretreatment baseline image is acquired at exactly the same position as the heating image. The MR acquisition can be triggered to a specific timepoint in the respiratory or cardiac cycles, but this is extremely sensitive to variations in these cycles. An alternative method is to acquire many baseline images before treatment begins, at many points in the motion cycle. Then, for all heating images, the corresponding baseline image is found and used for the subtraction. This approach has been used for MR thermometry of both RF ablation [21]-[22] and FUS ablation [23]-[24] of the liver.

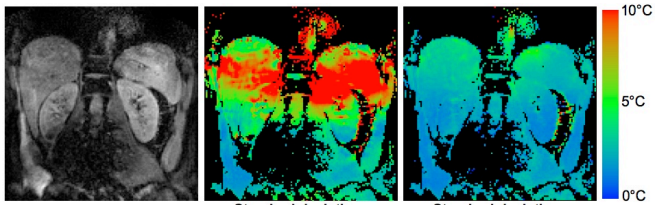

Fig. 3. Example images demonstrating the multibaseline approach to MR thermometry in the liver. (left) Anatomic image. The standard deviation of the temperature without correction (middle) and with correction (right) demonstrate the improvement. Images Courtesy of Baudouin Denis de Senneville and the Laboratory for Molecular and Functional Imaging, Universite Victor Segalen Bordeaux, Bordeaux, France.

C. Real-time Referenceless Methods

An alternative is to estimate the background phase (baseline data) from each heating image itself, which is a method called referenceless [25]-[26] or self-referenced thermometry [27].

We are using referenceless thermometry in conjunction with real-time imaging at 2.73 frames/s for thermometry in the liver. Phantom studies have been performed with the phantom moving in the MR scanner in a manner similar to

respiratory motion, as shown in Fig. 4. The depiction of the hotspot is maintained, as shown in Fig. 5. *In vivo* imaging demonstrates that there are no erroneous pixels exhibiting an apparent heat rise above the temperature threshold of 5°C.

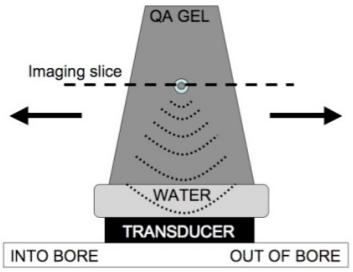

Fig. 4. Phantom setup to simulate respiratory motion of the liver, with the phantom moving approximately sinusoidally at 13 mm/s. The InSightec FUS transducer in this setup moves with the phantom.

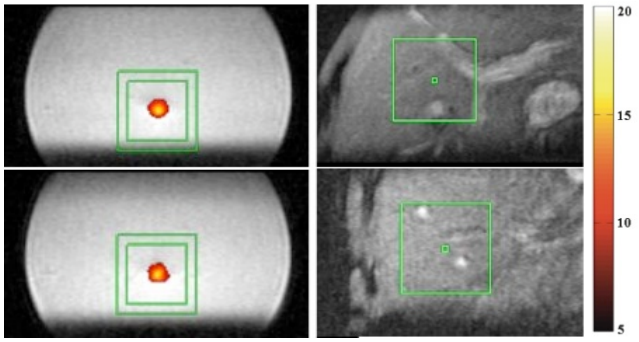

Fig. 5. Real-time MR thermometry at 2.73 frames/s with a multishot readout-segmented EPI sequence, reduced field of view with in-plane saturation bands, spatial-spectral RF excitation, and referenceless processing. (left) The phantom data demonstrates outstanding depiction of the hotspot, with temperature overlay threshholded at 5°C, when moving (lower left) compared to stationary (upper left). In vivo human imaging in the axial (upper right) and coronal (lower right) scan planes, with temperature overlay threshholded at 5°C, demonstrates that there are no pixels that appear to have a temperature rise of more than 5°C.

D. Feedback and Control

In addition to the requirement that temperature images be free of artifacts, there is also a need to slew the ultrasound beam based on motion of the liver, in order to ensure a tight focus. This is an area of ongoing work. Another example of using MR images for feedback and control is demonstrated in Fig. 6. In this example, the ultrasound beam from a transurethral applicator is rotated and controlled to provide uniform heating on a prescribed boundary in the prostate [28].

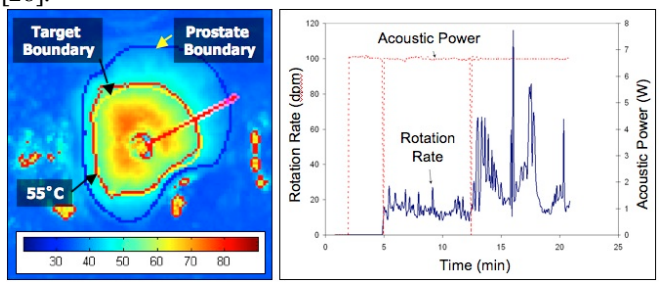

Fig. 6. (left) Real-time MR thermometry was used to control the shape of a spatial heating pattern generated in the canine prostate gland with transurethral high intensity ultrasound. A rotating transurethral heating applicator consisting of a planar transducer operating at 9.1 MHz was used in this experiment. The goal of the treatment was to elevate the temperature along the target boundary to 55°C. (right) The acoustic power and rotation rate required to produce this heating pattern is shown over the course of the 20 minute treatment. Image courtesy of Rajiv Chopra and Michael Bronskill.

IV. Assessment/Follow-Up

A. Limitations

After a thermal ablation treatment, it is useful to perform an immediate assessment of the treatment, to see if any areas need to be retreated, and to document the completeness of the treatment. MR assessment can be done with an intravenous infusion of a gadolinium contrast agent, which delineates the nonperfused volume. High resolution 3D contrast-enhanced (CE) imaging can then yield good quality images in a few minutes. An example CE image after transurethral ultrasound ablation is shown in Fig. 7. The drawback to the use of a contrast agent is that if the physician were to decide to retreat, he cannot then assess his second treatment with the same method, as the contrast agent will already be present.

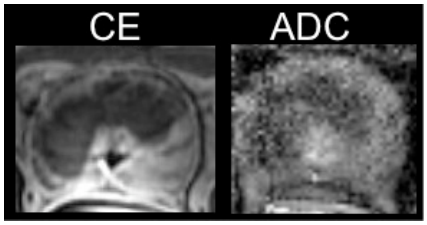

Fig. 7. Example contrast enhanced and apparent diffusion coefficient (ADC) maps of the same experiment shown in Fig. 1, demonstrating the same area treated by high intensity ultrasound.

B. DWI

As an alternative to CE imaging, we [29]-[31] and others [32] have shown a decrease in the apparent diffusion coefficient (ADC) after thermal ablation. The ADC map outlines the thermal lesion and can be conveniently repeated as needed. An example image of a thermal lesion created with ultrasound is shown in Fig. 7. The whole area of necrosis has a low ADC. The advantage of the DW method over the CE method is that it can be repeated if part of the target needs to be retreated.

A quantitative examination of the diffusion-weighted images across 19 ablated canine prostates, shown in Fig. 8, demonstrates a 36% drop in ADC in the ablated tissue, with no statistical difference between the ultrasound ablated and cryoablated tissues. Similar low ADC values have been found in uterine fibroids after ultrasound ablation [32, 33]. However, care must be taken when interpreting these images. The ADC values of cystic tissue may not change after the ablation, and other types of tissue, such as fibrotic tissue, may have a low ADC even before ablation.

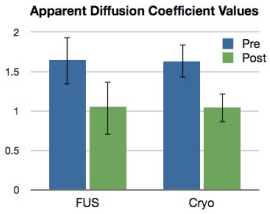

Fig. 8. The 36% drop in ADC across 19 canine prostate ablations did not depend on how the tissue was ablated.

C. Magnetization Transfer

Magnetization Transfer (MT) has been explored as a method to visualize FUS lesions, as it has been thought that changes in protein structure might be visible on MT images. The method uses an off-resonance pulse to protons in the macromolecules. The transfer of this energy saturates water protons. Our findings were that changes on MR images after ultrasound ablation in the prostate were visible several hours after ablation and remained as the tissue remodeled [34]. Therefore, at this point, this method appears more suited to long term assessment.

V. Conclusions

There are many challenges and exciting areas of ongoing research in MR-guided HIFU. Flexibility in image contrast mechanisms is allowing development of methods not only in temperature imaging, but also in the setup/calibration phase of the procedure and in the assessment and follow-up phase.

References

[1] De Poorter J. Noninvasive MRI thermometry with the proton resonance frequency method: study of susceptibility effects. *Magn Reson Med.* 1995 Sep;34(3):359–367.

[2] De Poorter J, De Wagter C, De Deene Y, Thomsen C, Stahlberg F, Achten E. Noninvasive MRI thermometry with the proton resonance frequency (PRF) method: in vivo results in human muscle. *Magn Reson Med.* 1995 Jan;33(1):74–81.

[3] Peters RD, Hinks RS, Henkelman RM. Ex vivo tissue-type independence in proton-resonance frequency shift MR thermometry. *Magn Reson Med.* 1998 Sep;40(3):454–459.

[4] Sapareto SA, Dewey WC. Thermal dose determination in cancer therapy. *Int J Radiat Oncol Biol Phys.* 1984 Jun;10(6):787–800.

[5] O'Sullivan AK, Thompson D, Chu P, Lee DW, Stewart EA, Weinstein MC. Cost-effectiveness of magnetic resonance guided focused ultrasound for the treatment of uterine fibroids. *Int J Technol Assess Health Care.* 2009 Jan;25(1):14–25.

[6] Rabinovici J, David M, Fukunishi H, Morita Y, Gostout B, Stewart E. Pregnancy outcome after magnetic resonance-guided focused ultrasound surgery (MRgFUS) for conservative treatment of uterine fibroids. *Fertil Steril.* 2008 Nov 13.

[7] Tempany CMC, Stewart EA, McDannold N, Quade BJ, Jolesz FA, Hynynen K. MR imaging-guided focused ultrasound surgery of uterine leiomyomas: a feasibility study. *Radiology.* 2003 Mar;226(3):897–905.

[8] Ferrara KW. Driving delivery vehicles with ultrasound. *Adv Drug Deliv Rev.* 2008 Jun 30;60(10):1097–1102.

[9] Tartis MS, McCallan J, Lum AFH, LaBell R, Stieger SM, Matsunaga TO, Ferrara KW. Therapeutic effects of paclitaxel-containing ultrasound contrast agents. *Ultrasound Med Biol.* 2006 Nov;32(11):1771–1780.

[10] Shortencarier MJ, Dayton PA, Bloch SH, Schumann PA, Matsunaga TO, Ferrara KW. A method for radiation-force localized drug delivery using gas-filled lipospheres. *IEEE Trans Ultrason Ferroelectr Freq Control.* 2004 Jul;51(7):822–831.

[11] Dayton PA, Allen JS, Ferrara KW. The magnitude of radiation force on ultrasound contrast agents. *J Acoust Soc Am.* 2002 Nov;112(5 Pt 1):2183–2192.

[12] Fry FJ, Ades HW, Fry WJ. Production of reversible changes in the central nervous system by ultrasound. *Science.* 1958 Jan 10;127(3289):83–84.

[13] Fry WJ. Intense ultrasound in investigations of the central nervous system. *Adv Biol Med Phys.* 1958;6:281–348.

[14] Hynynen K, McDannold N, Vykhodtseva N, Jolesz FA. Non-invasive opening of BBB by focused ultrasound. *Acta Neurochir Suppl.* 2003;86:555–558.

[15] Hynynen K, McDannold N, Vykhodtseva N, Jolesz FA. Noninvasive MR imaging-guided focal opening of the blood-brain barrier in rabbits. *Radiology.* 2001 Sep;220(3):640–646.

[16] McDannold N, Maier SE. Magnetic resonance acoustic radiation force imaging. *Med Phys.* 2008 Aug;35(8):3748–3758.

[17] Chen J, Watkins R, Butts Pauly K. Optimization of Encoding Gradients for Magnetic Resonance Acoustic Radiation Force Imaging. *ISMRM*; 2008 May.

[18] Hynynen K, Sun J. Trans-skull ultrasound therapy: the feasibility of using image-derived skull thickness information to correct the phase distortion. *IEEE Trans Ultrason Ferroelectr Freq Control.* 1999;46(3):752–755.

[19] Robson MD, Bydder GM. Clinical ultrashort echo time imaging of bone and other connective tissues. *NMR Biomed.* 2006 Nov;19(7):765–780.

[20] Urban MW, Bernal M, Greenleaf JF. Phase aberration correction using ultrasound radiation force and vibrometry optimization. *IEEE Trans Ultrason Ferroelectr Freq Control.* 2007 Jun;54(6):1142–1153.

[21] Vigen KK, Jarrard J, Rieke V, Frisoli J, Daniel BL, Butts Pauly K. In vivo porcine liver RF ablation with simultaneous MR temperature imaging. *J Magn Reson Imaging.* 2006 Apr;23(4):578–584.

[22] Vigen KK, Daniel BL, Pauly JM, Butts K. Triggered, navigated, multi-baseline method for proton resonance frequency temperature mapping with respiratory motion. *Magn Reson Med.* 2003 Nov;50(5):1003–1010.

[23] de Senneville Baudoin Denis, Quesson B, Desbarats P, Salomir R, Palussiere J, Moonen CTW. Atlas-based motion correction for on-line MR temperature mapping. *IEEE, ICIP*; 2004.

[24] de Senneville BD, Mougenot C, Moonen CTW. Real-time adaptive methods for treatment of mobile organs by MRI-controlled HIFU. *Magn Reson Med.* 2007 Feb;57(2):319–330.

[25] Rieke V, Vigen KK, Sommer G, Daniel BL, Pauly JM, Butts K. Referenceless PRF shift thermometry. *Magn Reson Med.* 2004 Jun;51(6):1223–1231.

[26] Grissom WG, Lustig, M, Rieke V, Holbrook AB, Pauly JM, Butts Pauly K. Referenceless MR Thermometry Using Iteratively-Reweighted L1 Regression. *ISMRM*; 2009.

[27] Kuroda K, Kokuryo D, Kumamoto E, Suzuki K, Matsuoka Y, Keserci B. Optimization of self-reference thermometry using complex field estimation. *Magn Reson Med.* 2006 Oct;56(4):835–843.

[28] Chopra R, Baker N, Choy V, Boyes A, Tang K, Bradwell D, Bronskill MJ. MRI-compatible transurethral ultrasound system for the treatment of localized prostate cancer using rotational control. *Med Phys.* 2008 Apr;35(4):1346–1357.

[29] Butts K, Daniel BL, Chen L, Bouley DM, Wansapura J, Maier SE, Dumoulin C, Watkins R. Diffusion-weighted MRI after cryosurgery of the canine prostate. Magnetic resonance imaging. *J Magn Reson Imaging.* 2003 Jan;17(1):131–135.

[30] Chen J, Daniel BL, Diederich CJ, Bouley DM, van den Bosch MAAJ, Kinsey AM, Sommer G, Pauly KB. Monitoring prostate thermal therapy with diffusion-weighted MRI. *Magn Reson Med.* 2008 Jun;59(6):1365–1372.

[31] Pauly KB, Diederich CJ, Rieke V, Bouley D, Chen J, Nau WH, Ross AB, Kinsey AM, Sommer G. Magnetic resonance-guided high-intensity ultrasound ablation of the prostate. *Top Magn Reson Imaging.* 2006 Jun;17(3):195–207.

[32] Jacobs MA, Herskovits EH, Kim HS. Uterine fibroids: diffusion-weighted MR imaging for monitoring therapy with focused ultrasound surgery--preliminary study. *Radiology.* 2005 Jul;236(1):196–203.

[33] Pilatou MC, Stewart EA, Maier SE et. al. MRI-based thermal dosimetry and diffusion-weighted imaging of MRI-guided focused ultrasound thermal ablation of uterine fibroids. *J Magn Reson Imaging.* 2009 Feb;29(2):404–411.

[34] Holbrook A Holbrook A, Bouley D, Alley M, Daniel B, Diederich C, Sommer G, Butts Pauly K. In vivo assessment of canine prostate thermal ablations with magnetization transfer imaging. *ISMRM*; 2007.